MONODEUTERATED METHANE: AN ISOTOPIC PROBE TO MEASURE BIOLOGICAL METHANE METABOLISM RATES AND TRACK CATABOLIC EXCHANGE REACTIONS

Jeffrey J. Marlow[1*#], Joshua A. Steele[1^], Wiebke Ziebis[2], Silvan Scheller[1], David Case[1], Victoria J. Orphan[1]

[1] Division of Geological and Planetary Sciences, California Institute of Technology, Pasadena, CA, 91125 USA
[2] Department of Biological Science, University of Southern California, Los Angeles, CA, 90089 USA
* Current address: Dept. of Organismic and Evolutionary Biology, Harvard University, Cambridge, MA 02138 USA
^ Current address: Southern California Coastal Water Research Project, Costa Mesa, CA 92626 USA
# Correspondence email: marlow@fas.harvard.edu

Abstract

Biological methane oxidation is a globally relevant process that mediates the flux of an important greenhouse gas through both aerobic and anaerobic metabolic pathways. However, measuring the rates of these metabolisms presents many obstacles, from logistical barriers to regulatory hurdles and poor precision. Here we present a new approach for measuring rates of microbial methane metabolism, using monodeuterated methane (CH_3D) as a metabolic substrate and quantifying the change in the aqueous D/H ratio over time using off-axis integrated cavity output spectroscopy. This method represents a non-toxic, comparatively rapid and straightforward approach that is complementary to existing radio- (^{14}C) and stable (^{13}C) carbon isotopic methods; by probing hydrogen atom dynamics, it offers an additional dimension through which to examine the rates and pathways of methane metabolism. We provide direct comparisons between the CH_3D procedure and the well-established $^{14}CH_4$ radiotracer method for several methanotrophic systems, including type I and type II aerobic methanotroph cultures – for which the new approach is five times more precise – and methane seep sediment and carbonate rocks under anoxic and oxic incubation conditions. We also employ this method in a non-traditional experimental set-up, investigating the role of pressure on methane oxidation rates in anoxic seep sediment. Results revealed an 80% increase in methanotrophic rates at the equivalent of ~900 m water depth (40 MPa), revealing an important environmental parameter for methane metabolism and exhibiting the flexibility of the newly described method.

The monodeuterated methane approach offers a procedurally straightforward, reliable method that advances three specific aims. First, it allows users to directly compare methanotrophic rates between different experimental treatments of the same inoculum. Second, by empirically linking the CH_3D procedure with the well-established ^{14}C-radiocarbon approach, an absolute

scaling factor can be determined for new systems of interest. This "ground-truthing" strategy enables "CH_3D only" experiments to yield rates of full methane oxidation; we demonstrate this principle in the context of several methanotrophic systems. Finally, monodeuterated methane facilitates a continued evaluation of C- and H-atom tracking through methanotrophic metabolisms, with specific foci on enzyme reversibility and anabolic/catabolic branch points. The procedural advantages, consistency, and novel research questions enabled by the monodeuterated methane method should prove useful in a wide range of culture-based and environmental microbial systems to further elucidate methane metabolism dynamics.

1. Introduction

Methane-consuming microbial processes represent an important component of biogeochemical cycles in natural freshwater and marine environments, as well as in human-impacted systems. In terrestrial soils, methane production in rice fields, anoxic wetlands, and thawing permafrost supports methanotrophic communities (Holzapfel-Pschorn et al., 1985; Mackelprang et al., 2011). In marine settings, an estimated 85 Tg of methane per year, derived from biogenic and thermogenic sources, enters the subseafloor, the vast majority of which is anaerobically consumed in anoxic sediments (Reeburgh, 2007). Much of what remains is taken up in microoxic or oxic zones of the sediment or water column by aerobic methanotrophic microorganisms (Valentine et al., 2001). In freshwater wetlands, approximately 200 Tg of methane is generated per year, most of which is oxidized by hydroxyl radicals in the troposphere (Kirschke et al., 2013). Methanotrophy is also of interest in a range of human-impacted contexts, including wastewater treatment plants (Ho et al., 2013), landfills (Scheutz et al., 2009), and oil spills (Crespo-Medina et al., 2014).

In addition to the climatic and economic implications of the methanotrophic process, its biochemical details have stimulated many investigations. The anaerobic oxidation of methane (AOM) has proven particularly enigmatic, often involving a mutualistic relationship between anaerobic methanotrophic (ANME) archaea and sulfate reducing bacteria (SRB; Boetius et al., 2000; McGlynn et al., 2015; Scheller et al., 2016; Wegener et al., 2015). A consensus on the precise nature of the mutualism remains outstanding, but the net result of the process is typically the stoichiometric oxidation of methane coupled with sulfate reduction (Knittel and Boetius, 2009). Alternative electron acceptors including nitrate (Haroon et al., 2013), and nitrite (Ettwig et al., 2010) have been demonstrated, while several studies have presented equivocal evidence for methane oxidation coupled directly to iron or manganese reduction (Beal et al., 2009; Nauhaus et al., 2005; Sivan et al., 2014).

Methane is oxidized aerobically by members of the classes *Gammaproteobacteria* (Type I) and *Alphaproteobacteria* (Type II); verrucomicrobial representatives were more recently found to perform aerobic methanotrophy under extremely acidic conditions (Dunfield et al., 2007; Op den Camp et al., 2009). Methane monooxygenase converts methane to methanol, which is further oxidized to formaldehyde; assimilatory pathways branching at this point can incorporate carbon into central metabolism through the ribulose monophosphate (RuMP) cycle (Type I methanotrophs) or the serine cycle (Type II). Remaining formaldehyde can undergo two additional oxidation reactions, being converted first to formate and ultimately to carbon dioxide (Hakemian and Rosenzweig, 2007).

Methanotrophy is both a biogeochemically relevant force that modulates global climate and a poorly understood biochemical process; given this dual role, there is substantial interest in measuring the rate of the process and understanding elemental flows through metabolic pathways.

75 The oxidation of methane in environmental samples has traditionally been studied using a handful
76 of techniques. Numerical models incorporating environmental sediment profiles of sulfate and
77 methane concentrations can be used to back-calculate methane consumption rates (Jørgensen et al.,
78 2001). Methane labeled with ^{13}C can be used to probe longer-term rates in controlled conditions
79 (Moran et al., 2008), but the presence of natural ^{13}C in marine dissolved inorganic carbon pools
80 requires long incubations as well as accurate measurements of concentrations and isotopic
81 compositions of reactants and products (Pack et al., 2011). Gas chromatography quantification of
82 dissolved (Girguis et al., 2003) or headspace (Carini et al., 2003) methane concentrations has also
83 been demonstrated as a rate measurement tool, though low concentrations can hamper
84 reproducibility and exacerbate background contamination issues, particularly in field-based
85 settings (Magen et al., 2014). Perhaps the most sensitive approach uses radiolabeled $^{14}CH_4$ to track
86 the oxidation of methane-associated carbon to inorganic carbon species (Alperin and Reeburgh,
87 1985; Treude et al., 2003). Labeling with tritiated methane was introduced for water column
88 aerobic methane oxidation measurements due to its higher specific activity and the procedural
89 advantages of working with a water-phase product rather than gaseous products (Bussmann et al.,
90 2015; Valentine et al., 2001). Logistical challenges and health and safety regulations led Pack et al.
91 (2011) to develop an accelerator mass spectrometry detection method that requires 10^3-10^5 less
92 radiolabel than previous ^{14}C and ^{3}H approaches, though the analytical procedure remains labor
93 intensive.
94 Despite the range of methods available, measurement of microbial methane utilization rates
95 remains cumbersome, and the demonstration of a precise, safe, and easily enacted approach would
96 be a welcome contribution for a diverse field of researchers. Nearly all of the aforementioned
97 approaches are carbon-based; a hydrogen-based tracer offers an additional dimension to

98 investigations of methane biochemical dynamics. Here we introduce a novel method for
99 biologically mediated methanotrophy rate measurement that utilizes monodeuterated methane
100 (CH_3D) as a substrate and measures the D/H ratio of the aqueous solution.
101 We demonstrate, through methanotrophic cell cultures and microcosm incubations of
102 seafloor sediment and carbonate rock fragments, that methane activation rates derived from
103 aqueous D/H values are consistently proportional to ^{14}C-based methane oxidation rate
104 measurements for the laboratory treatments tested in this study. The resulting ratios, when viewed
105 in the context of partial (methane-associated hydrogen exchange) versus complete methane
106 oxidation (methane oxidation to CO_2), represent a new tool with which to examine the reversibility
107 and catabolic / anabolic partitioning of methanotrophic metabolisms. As a proof of concept, we
108 apply the monodeuterated methane approach to pressurized methane seep sediment incubations in
109 order to test the role of an understudied environmental variable in methanotrophic rates under non-
110 traditional empirical conditions. As a rate measurement protocol, this approach offers several
111 advantages over current techniques: it does not require the logistical, safety, and administrative
112 hurdles associated with radiotracers such as $^{14}CH_4$ and ^{3}H-CH_4, it is less susceptible to analyte loss
113 than methane headspace measurements, and compares favorably in terms of equipment cost and
114 portability.
115
116 **2. Methods**
117 2.1. Experimental Set-Up
118 To demonstrate the precision and reproducibility of the monodeuterated methane approach,
119 it was tested alongside the well-established $^{14}CH_4$ radiotracer protocol. The use of $^{14}CH_4$ is an
120 accepted standard procedure in studies of methane consumption quantification (e.g., Knittel and

Boetius, 2009; Ruff et al., 2016; Segarra et al., 2013) and has been experimentally cross-referenced with methane concentration measurements (Treude et al., 2003) and other approaches including tritiated methane techniques (Mau et al., 2013; Pack et al., 2011). Both techniques were applied to a) aerobic methanotrophic cultures of *Methylosinus trichosporium OB3b* (kindly supplied by Marina Kalyuzhnaya and Mary Lidstrom) and *Methyloprofundus sedimenti* (isolated from a deep sea whale fall; Tavormina et al., 2015) b) oxic incubations of methane seep sediment and carbonate rocks, and c) anoxic incubations of methane seep sediment and carbonate rocks. In addition, the monodeuterated methane protocol was employed in a pressure-based experiment to demonstrate the technique's adaptability to distinct empirical set-ups and examine the relative effect of heightened, environmentally relevant pressure on methane consumption rates in anoxic seep sediment samples. Monodeuterated methane for all samples was 98% pure CH_3D obtained from Sigma-Aldrich ($247 / L). For a representation of all experiments conducted in this study, see Table 1.

2.1.1. Experiments with Aerobic Methanotroph Cultures

Cultures of *Methylosinus trichosporium* strain OB3b (Whittenbury et al., 1970) were grown using Nitrate Mineral Salts (NMS) medium at 30 °C. The newly characterized *Methyloprofundus sedimenti* strain WF1 was grown in a modified NMS medium at 25 °C (Tavormina et al., 2015). In both cases, shaking cultures were grown up from stock in sealed 25 mL test tubes that contained 5 mL media and 50:50 air:methane by volume. After several successful transfers (as determined by an increase in optical density, data not shown), experiments were initiated by passaging 0.94 mL of exponential phase inoculum into 8.5 mL media, for each of ten different experimental conditions, each prepared in triplicate (see Table S1). Due to the

143 destructive nature of the $^{14}CH_4$ method, three of these triplicate sets were used to measure methane
144 oxidation at three distinct time points.
145 Samples for D/H analysis were taken at seven time points throughout 140-hour (*M.*
146 *trichosporium*) and 476-hour (*M. sedimenti*) experiments. Sampling points were most concentrated
147 around anticipated exponential growth phases as determined by optical density (600 nm) profiles
148 of earlier rounds of culture transfers. Samples for radiolabel processing were taken at 46, 102, and
149 166.5 hours for *M. trichosporium* cultures and 102, 166.5, and 432 hours for the slower-growing
150 *M. sedimenti* cultures. Killed, cell-free, oxygen-free, and CH_3D-free controls were all assessed
151 (Table S1).
152 *2.1.2. Experiments with Environmental Samples: Methane Seep Sediments and Carbonates*
153 Samples recovered from the Hydrate Ridge methane seep system were used to
154 comparatively examine the novel monodeuterated methane (CH_3D) approach alongside the $^{14}CH_4$
155 protocol with environmental samples. Hydrate Ridge, Oregon, is located along a convergent
156 tectonic margin and is well established as a site of methane seepage and sediment-based AOM
157 (e.g., Suess et al., 1999; Treude et al., 2003; Tryon et al., 2002). Methane concentrations within the
158 most active seep sediments reach several mM, and have been measured and modeled at values up
159 to 70 mM (Boetius and Suess, 2004) and 50 mM (Tryon et al., 2002) respectively.
160 Samples were collected with the Deep Submergence Vehicle (DSV) *Alvin* during *Atlantis*
161 leg AT-16-68 in September 2010 and the Remotely Operated Vehicle (ROV) *Jason* II during
162 *Atlantis* leg AT-18-10 in September 2011; materials used for methanotrophic rate experiments are
163 specified in Table 1. The "active" designation in our sample descriptions refers to sites where
164 methane seepage was manifested by seafloor ecosystems known to be fueled by subsurface
165 methane (e.g. clam beds and microbial mats) or methane bubble ebullition. The term "low activity"

166 references sampling sites that did not exhibit any clear signs of contemporary methane seepage or
167 chemosynthetic communities, though a small amount of methane supply and methanotrophic
168 potential cannot be ruled out as subsurface advective flow can shift with time (Gieskes et al., 2005;
169 Marlow et al., 2014; Tryon et al., 2002). Sample types are abbreviated by the A.Sed (active
170 sediment), A.Carb (active carbonate), L.Sed (low-activity sediment), and L.Carb (low-activity
171 carbonate) designations. Seven samples were analyzed to examine a range of physical substrate
172 type (sediment vs. carbonate rock) and seepage environments (active and low-activity): A.Sed-
173 5128, A.Carb-5305, A.Carb-5152, L.Sed-5043, L.Carb-5028, and sterilized control aliquots of
174 A.Sed-5128 and A.Carb-5305. Carbonate samples include both porous materials with macroscale
175 vugs and pore spaces, as well as massive lithologies with more homogenous structure.
176 Shipboard, push cores and bottom water-submerged carbonates were immediately
177 transferred to a 4 °C walk-in cold room and processed within several hours. To prepare material for
178 future experimentation, sediment and carbonate rocks were stored in anoxic, Ar-flushed, gas-tight
179 mylar bags (Impak Corp., Los Angeles, USA) at 4 °C until use several months later. In advance of
180 experimental set-up, carbonate samples and homogenized sediment from the 0-12 cm push core
181 horizon were prepared under anoxic conditions using 0.22 μm-filtered, anoxic N_2-sparged Hydrate
182 Ridge bottom water (at a 1:2 sediment/carbonate:bottom water ratio by volume). Samples were
183 maintained under a $2x10^5$ Pa CH_4 headspace for one month in order to resuscitate activity; the
184 corresponding dissolved concentration (3.7 mM) is consistent with environmental methane
185 concentrations at Hydrate Ridge (Boetius and Suess, 2004).
186 To set up the experimental incubations, 10 mL physical substrate (compressed sediment or
187 carbonate rock) and 20 mL filtered Hydrate Ridge bottom water were placed in 60-mL glass
188 bottles (SVG-50 gaschro vials, Nichiden Riku Glass Co, Kobe, Japan). In all experiments

involving carbonates, interior portions (> 5 cm from the rock surface) were used in order to ensure that properties exhibited were representative of bulk rock material and not a reflection of surface-based adherent cells or entrained material. Carbonate rock samples were fragmented in order to fit through the 28-mm diameter bottle opening; pieces were kept as large as possible to minimize the increase in surface area-to-volume ratio and maintain conditions as representative of the *in situ* environment as possible. All bottles were sealed with butyl stoppers; following several minutes of flushing with N_2 (g), the headspace was replaced with methane, and an additional 30 mL of gas, whose composition varied depending on the experiment, was injected into the 30 mL headspace to generate an absolute pressure of approximately $2x10^5$ Pa. Anoxic incubation headspace was 100% methane; oxic incubation headspace was 30 mL methane, 20 mL N_2, and 10 mL O_2. All incubation set-up prior to gas flushing and headspace injection took place in an anaerobic chamber. Triplicate samples, including killed controls, were prepared for all sample types. Measurements were taken for both D/H and ^{14}C analysis at 46 and 96 hours for oxic incubations, and 72 and 192 hours for anoxic incubations. Anoxic active methane seep sediment (A.Sed-5128) incubations were used for nuclear magnetic resonance (NMR) analysis of the remaining methane (set up in triplicate, with 60 mL CH_3D initial headspace) as well as empirical resolution studies sampled between days 20-22.

2.1.3. Experiments with Environmental Samples in Pressure Vessels

In order to probe the effect of pressure on anaerobic methanotrophic rates, a set of experiments was established, using the monodeuterated methane technique to determine relative rate differences. Active sediment from Hydrate Ridge (A.Sed-3450) was collected from a water depth of 850 m and an ambient temperature of 4 °C, processed shipboard, and prepared for experimentation as described above. To set up the incubations, eight 100 mL mylar bags were prepared with the components shown in Table S2 using homogenized sediment from the 0-12 cm

horizon. 500 μM glycine or 500 μM ammonium were added in order to evaluate relative rate differences associated with organic and inorganic sources of nitrogen. Identical sets of four compositionally distinct samples – including killed controls – were established such that each treatment could be subjected to low pressure (0.1 MPa, i.e., atmospheric pressure) and high pressure (9.0 MPa, equivalent to ~900 m water depth). Prior to gas addition, each bag was flushed for 5 min. with Ar.

The use of flexible mylar bags is essential for the application of external pressure, yet it presents obstacles for "traditional" methanotrophic rate measurement protocols such as the $^{14}CH_4$ method. In particular, the processing of post-incubation headspace is optimized for stoppered bottles, and accessing the gas phase from mylar bags in a quantitative fashion is challenging. Measurement of radiolabeled dissolved inorganic carbon requires that all incubation material be transferred to an Erlenmeyer flask equipped with a scintilation vial; sediment grains are commonly trapped in the seals of mylar bags, complicating this transfer. For these reasons, monodeuterated methane addition and subsequent aqueous measurement offered a useful tool for this challenging experimental set-up.

Once the incubations were prepared, they were transported to the laboratory of Dr. William Berelson at the University of Southern California and placed in a walk-in cold room (4 °C). Incubations for pressurized treatment were inserted into a stainless steel, custom-built pressure chamber with 3-cm thick walls and pressure valves rated to 40 MPa, and hydraulic fluid was pumped into the sealed chamber using a Star Hydraulics P1A-250 hand pump. The pressure was maintained at 9.0 MPa during the course of the 38-day experiment, with daily adjustments to account for thermal compression effects. At the conclusion of the experiment, mylar bags were removed from the chamber, checked for leaks (none were observed, as the bags were still inflated,

the seal was still gas-tight, and no hydraulic fluid was detected in the interior of the mylar bags) and sampled for D/H ratio measurement.

2.2. Analytical Procedures

2.2.1. Rate Measurements Derived from CH_3D Addition

At designated sampling times, 1 mL of medium / water was collected from cultures or incubations in an anaerobic chamber with a sterile syringe. A constant volume was maintained by adding 1 mL of sterile media immediately after sampling; this media was previously equilibrated with gaseous headspace specific to each experiment. Sampled liquid was then pushed through a 0.22 μm Durapore filter (EMD Millipore, Temecula, CA) and into a 1-mL GC vial. A LGR DLT-100 liquid water isotope analyzer (LWIA, Los Gatos Research, Mountain View, CA) was used to determine the D/H ratio of each sample. The LWIA uses off-axis integrated-cavity output spectroscopy to measure isotopically specific absorption patterns and determine simultaneous D/H and $^{18}O/^{16}O$ ratios with high precision and robust mechanics (Lis et al., 2008). Such instruments have been used for a range of studies, including hydrological analysis (Robson and Webb, 2016), mine waste management (Huang et al., 2015), and microbial metabolism (Dawson et al., 2015).

In this study, an injection volume of 700 nL at 1000 nL/s was used, with four intra-injection flush strokes and a flush time of 60 s between injections. Four rounds of ten injections per sample were performed in order to avoid memory effects; only the latter five injections were used in subsequent calculations. Sample runs were limited to ~250 injections in order to minimize salt precipitation, and each analysis included an appropriate blank (i.e., autoclaved media for the cultures, or filter sterilized bottom water used during incubation set-up in the case of sediment and carbonate incubations) and two standards of known isotopic ratios (Deep Blue: $\delta D = 0.5‰$, and CIT: $\delta D = -73.4‰$). Data was removed if instrumental temperature or pressure parameters were

observed to fall outside of optimal instrument specifications (0.76% of all analyses), corresponding to an internal temperature change of more than 0.3 °C per hour or rising pressure within the measurement cell during the analysis.

To calculate methane consumption rates, D/H ratios from the LWIA were first normalized to the Vienna standard mean ocean water (VSMOW) scale using a two-point calibration from the water standards and a linear interpolation (e.g., Dawson et al., 2015). To minimize the effects of instrumental drift, standards were re-measured between rounds of sample analysis (maximum of 40 injections) and new scaling factors were implemented. The number of total hydrogen atoms (H and D) present at the initial time point was calculated using the experiment's overall water volume, as in equation 1:

$$\frac{vol(L)}{1} * \frac{55.5\ mol\ water}{L} * \frac{6.022\ x\ 10^{23}\ molecules\ water}{mol\ water} * \frac{2\ hydrogen\ atoms}{molecule\ water} = hyd.atoms\ in\ inc._{T1}$$

The number of D atoms newly present in the experiment's aqueous phase between time points T_1 and T_2 was determined using the normalized D/H values, averaging across the latter five injections of the four distinct injection rounds; see equations 2.1-2.3:

$$\left[\left(\frac{D}{H}\right)_{T2} * (hyd.atoms\ in\ inc.)_{T2}\right] - \left[\left(\frac{D}{H}\right)_{T1} * (hyd.atoms\ in\ inc.)_{T1}\right] = new\ D\ atoms\ in\ inc.$$

$$(hyd.atoms\ in\ inc.)_{T2} \approx (hyd.atoms\ in\ inc.)_{T1}$$

$$\left[\left(\frac{D}{H}\right)_{T2} - \left(\frac{D}{H}\right)_{T1}\right] * (hyd.atoms\ in\ inc.)_{T1} = new\ D\ atoms\ in\ inc. = D_{new}$$

D_{new} was multiplied by four given the 1:3 D:H stoichiometry of the CH_3D substrate to derive the maximum number of methane molecules consumed catabolically through initial C-X bond activation (equation 3).

$$D_{new} * 4 = maximum\ number\ of\ methane\ molecules\ consumed = C$$

The scaling factor of four was used in the context of methane activation – the initial mobilization through conversion to a methyl group – to calculate the maximum number of methane molecules that could be consumed but not necessarily fully oxidized. This represents an end-member case that may not be appropriate for all subsequent processing as hydrogen/deuterium atoms are incorporated into biomass or exchanged. Caveats and potential interpretations of the absolute numbers that result from these calculations are discussed below, but we stress that with consistent implementation of scaling factors from comparisons between monodeuterated and radiolabel methods, rates derived from *C* and downstream parameters are valid and useful.

C was corrected based on the fraction of incubation methane headspace composed of CH_3D, yielding C_{corr}, as shown in equation 4:

$$\frac{C}{fraction\ of\ methane\ headspace\ that\ is\ CH3D} = C_{corr}$$

By dividing C_{corr} by the incubation time and volume, a maximum rate of methane consumption is determined (equation 5.1-5.2):

$$C_{corr} * \frac{mol}{6.022\ x\ 10^{23}\ molecules} * \frac{10^9\ nmol}{mol} * \frac{1}{incubation\ time\ (d)} * \frac{1}{incubation\ vol\ (cm^3)} = R_{CH3D}$$

$$R_{CH3D} = Maximum\ rate\ of\ methane\ consumption\ in\ \frac{nmol}{cm^3\ d}$$

2.2.2. Rate Measurements Derived from $^{14}CH_4$ Addition

Methane oxidation rates using radiolabeled methane substrate were measured as described in detail by Treude et al. (2005) and Treude and Ziebis (2010). Radiolabeled methane ($^{14}CH_4$ dissolved in seawater, corresponding to an activity of 13 kBq for culture experiments and 52 kBq in sediment and carbonate samples) was injected into each sample container, and samples were incubated at the appropriate temperatures for the designated amount of time (see above). To stop microbial activity and begin analysis, 2.5 ml of 2.5% NaOH was injected. Sample headspace was

293 flowed through a Cu^{2+} oxide-filled 850 °C quartz tube furnace, combusting unreacted $^{14}CH_4$ to
294 $^{14}CO_2$. This $^{14}CO_2$ was collected in two scintillation vials (23 ml volume) pre-filled with 7 ml
295 phenylethylamine and 1 ml 2-methoxyethanol, to which 10 ml of scintillation cocktail (Ultima
296 Gold XR, PerkinElmer) was added. After a 24-hour incubation period, radioactivity from $^{14}CO_2$
297 was measured by scintillation counting (Beckman Coulter LS 6500 Multi-Purpose Scintillation
298 Counter, 10 minute analysis per sample).
299 Labeled ^{14}C-inorganic carbon produced during the incubation was quantified as follows.
300 The entire volume of each incubation sample was transferred into a 250-ml Erlenmeyer flask along
301 with 1 drop of antifoam and 5 ml of 6M HCl. The flask was immediately stoppered and sealed
302 with two clamps and parafilm wrapping to prevent gas escape, and placed on a shaking table (60
303 rpm, room temperature, 24 hours). To collect $^{14}CO_2$ generated by the acidification process, a 7-ml
304 scintillation vial was pre-filled with 1 ml of 2.5% NaOH and 1 ml of phenylethylamine and
305 suspended from the rubber stopper inside the flask. After the shaking / acidification step, 5 ml of
306 scintillation cocktail was added, and the vial was measured by scintillation counting after 24 hours.
307 This method has been demonstrated to recover 98% of $^{14}CO_2$ on average (Treude et al., 2003).
308 Finally, sterilized control samples (#10, see Table S1) were set aside after $^{14}CH_4$ addition
309 for gas chromatography to determine the initial concentration of methane gas. 400 µl of headspace
310 was injected into a gas chromatograph (Shimadzu GC-2014), equipped with a packed stainless
311 steel Supelco Custom Column (50/50 mixture, 80/100 Porapak N support, 80/100 Porapak Q
312 column, 6 ft x 1/8 in) and a flame ionization detector. The carrier gas was helium at a flow rate of
313 30 ml min^{-1}, and the column temperature was 60 °C. Results were scaled based on comparison
314 with standards of known methane concentrations (10 and 100 ppm; Matheson Tri-Gas, Twinsburg,
315 OH). The rate of methane oxidation was determined by equation 6:

316 $$Methane\ Oxidation = \frac{^{14}CO_2 \bullet CH_4}{(^{14}CH_4 + ^{14}CO_2) \bullet v \bullet t}$$

317 in which $^{14}CH_4$ is the combusted unreacted radiolabeled methane, $^{14}CO_2$ represents the quantity of
318 acidified oxidation product, CH_4 signifies the initial quantity of methane in the experiment, v is the
319 volume of sediment or carbonate rock, and t is the time over which the incubation was active.

320 *2.2.3. Isotopic Analysis of Methane in the Headspace*

321 The methane headspace was analyzed via ^{1}H-NMR spectroscopy using a Varian 400 MHz
322 Spectrometer with a broadband auto-tune OneProbe. 300 µl of headspace was passed through
323 $CDCl_3$ with a fine needle to absorb the methane. ^{1}H-NMR spectra were acquired at 298 K without
324 spinning, using a repetition rate of 10 s to ensure reliable quantification. The spectra were
325 simulated with the iNMR 4.1.7 software for the determination of the fractional abundances of the
326 $^{12}CH_4$, $^{12}CH_3D$, $^{13}CH_4$ and $^{13}CH_3D$ isotopologs.

327

328 **3. Results and Discussion**

329 3.1. Comparison of CH_3D and $^{14}CH_4$ Rate Measurements in Aerobic Methanotroph Cultures

330 D/H ratios were acquired and corresponding C_{corr} values were calculated at eight points
331 during the *M. trichosporium* growth curve and seven points of the *M. sedimenti* growth curve.
332 Three measurements of ^{14}C distributions were acquired for each strain, targeting exponential and
333 stationary phases (Fig. 1). The Type II alphaproteobacterial methanotroph *M. trichosporium*
334 exhibited methane consumption rates more than an order of magnitude greater than those of *M.*
335 *sedimenti* (gammaproteobacterial Type I methanotroph), yet the scaling factor relating the CH_3D-
336 and $^{14}CH_4$-derived rates was remarkably consistent in both cases. Scaling factors were calculated
337 for both exponential growth and stationary phase, using data points from both CH_3D and $^{14}CH_4$
338 experiments. For example, the *M. trichosporium* rate value calculated from CH_3D experimental

339 treatment point (47.5 hours, 4.16 x 10^4 nmol methane consumed) was compared with the rate
340 determined from $^{14}CH_4$ experimental treatment point (47.5 hours, 2.77 x 10^4 nmol methane
341 consumed), yielding a scaling factor of 1.5 for exponential phase growth. Similarly, data from (140
342 h, 5.27 x 10^4 nmol, CH_3D) and (166.5 h, 4.24 x 10^4 nmol, $^{14}CH_4$) were used for *M. trichosporium*'s
343 stationary phase scaling factor. Equivalent values were determined for *M. sedimenti* using the
344 following data points: (140 h, 7.07 x 10^3 nmol, CH_3D) and (102 h, 3.43 x 10^3 nmol, $^{14}CH_4$) for the
345 exponential growth phase, and (476 h, 7.53 x 10^3 nmol, CH_3D) and (432 h, 4.30 x 10^3 nmol,
346 $^{14}CH_4$) for stationary phase.

347 In this way, the ratio of methane consumption rates derived from the CH_3D method (using
348 equations 1-5) and the $^{14}CH_4$ method (using equation 6) can be compared. This value is hereafter
349 referred to as the "D:^{14}C tracer ratio". This ratio can be used to evaluate the consistency of the
350 monodeuterated methane method compared with the well-established $^{14}CH_4$ approach, and as an
351 investigatory tool in catabolic / anabolic processing of methane (see "Understanding the D:^{14}C
352 Tracer Ratio", below).

353 D:^{14}C tracer ratio values were calculated for aerobic methanotroph cultures using the data
354 specified above and are shown in Table 2; their consistency is a promising indicator of the utility
355 of the monodeuterated methane approach for ground-truthed rate measurements. By dividing rates
356 derived from D/H values by 1.5, a reliable estimate of full-oxidation methanotrophy – that is, the
357 complete biological oxidation of methane to carbon dioxide – can be assessed.

358 3.2. Comparison of CH_3D and $^{14}CH_4$ Rate Measurements in Environmental Methane Seep Samples

359 Methane consumption rates under oxic microcosm incubation conditions, derived from
360 both CH_3D and $^{14}CH_4$ measurements, are provided for all five sample types (active sediment, low-
361 activity sediment, active porous carbonate, active massive carbonate, and low-activity massive

362 carbonate) in Fig. 2a. The corresponding values for anoxic conditions are shown in Fig. 2b. Values
363 were calculated from data collected after 4 days of incubation for oxic samples and after 8 days of
364 incubation for anoxic samples.

365 The D:^{14}C tracer ratio for the oxic incubations was 1.66 +/- 0.02 SE and 1.99 +/- 0.04 SE
366 for anoxic conditions (Table 2). These relatively consistent values across physical substrate type
367 (sediment and carbonates of varying lithology) and collection site activity level (active and low-
368 activity) suggest an underlying metabolic basis of these D:^{14}C tracer ratio that is unperturbed by
369 physicochemical factors or relative activity levels.

370 To determine the minimum number of activated CH_3D molecules needed for analytical
371 detection, we assessed the length of time required to measure a differentiable D/H ratio.
372 Measurements were acquired at multiple time points between days 20 and 22 of a triplicate set of
373 A.Sed-5128 incubations. A resolvable signal of an enhanced D/H ratio was defined as data points
374 with non-overlapping confidence intervals, representing a 95% statistical probability that D/H
375 ratios were increased. Such differentiation seen at the 20-hour sampling time for two replicates and
376 the 26-hour sampling time for the other one (Fig. S1). Using the rate determined by the first 20
377 days as a baseline, this translates to a resolution of 4.5-6.2 μmol of fully oxidized methane based
378 on the D:^{14}C tracer ratio of 2.05 (Table 2).

379 3.3. Understanding the D:^{14}C Tracer Ratio

380 The CH_3D and $^{14}CH_4$ approaches quantify distinct aspects of methanotrophy; that is,
381 methane activation or complete conversion to CO_2, respectively. The $^{14}CH_4$ technique quantifies
382 the amount of ^{14}C – initially supplied as methane – that is fully oxidized and persists as soluble
383 species (HCO_3^-) or acid-labile precipitation products ($CaCO_3$). The CH_3D protocol, on the other
384 hand, reports the extent to which methane-derived hydrogen atoms are detected in water. Because

385 methane is an inert molecule, abiotic exchange between methane- and water-associated hydrogen
386 atoms is not expected. Indeed, D/H ratios in killed control experiments remained stable (e.g.,
387 exhibiting a value of 1.40×10^{-4} +/- 3.1×10^{-8} SE at T_{0d} and 1.40×10^{-4} +/- 2.9×10^{-8} SE at T_{140d}
388 during experimentation with *M. trichosporium*, data incorporated into Fig. 1a). The activation of
389 methane thereby indicates enzymatic functionalization, but the ultimate fate of each hydrogen atom
390 during methane oxidation is unclear.

391 The flow of methane-derived hydrogen atoms through anaerobic and aerobic
392 methanotrophic metabolisms was examined in an attempt to predictively evaluate the consequence
393 of monodeuterated methane reactions. Previously published reports were used to compile Figure 3
394 (Hallam et al., 2004; Thauer, 2011; Vorholt and Thauer, 1997) and Figure 4 (Lieberman and
395 Rosenzweig, 2004), which trace anaerobic and aerobic methane metabolisms, respectively, with a
396 specific focus on hydrogen atoms. In this context, our observations of relatively consistent but
397 distinct D:^{14}C tracer ratios for anaerobic and aerobic methanotrophy (Table 2) likely reflect
398 different aspects of the two metabolic pathways. In AOM, metabolite backflux (Holler et al., 2011)
399 may increase the D/H ratio; in aerobic methanotrophy, biomass growth represents a substantial
400 carbon and hydrogen shunt.

401 *3.3.1. The D:^{14}C Tracer Ratio in Anaerobic Methanotrophy*

402 AOM is depicted in Fig. 3 via the reverse methanogenesis pathway, which is believed to be
403 enacted by ANME based on genetic (Hallam et al., 2004) and proteomic (Marlow et al., 2016)
404 data. In this metabolic process, methyl-coenzyme M reductase (Mcr) activates methane and
405 generates methyl-CoM. A tetrahydromethanopterin molecule supplants CoM, and subsequent
406 carbon oxidation steps release hydrogen atoms into the medium. Ultimately, the number of
407 methane-derived hydrogen atoms that enter water-exchangeable products determines the

408 physiological interpretation of aqueous D/H ratios. For example, if just one methane-derived
409 hydrogen enters an intermediate and is freely exchangeable with water, then observed water-based
410 deuterium must be multiplied by four (to account for methane's hydrogen-carbon stoichiometry;
411 see equation 3) and a primary isotope effect as high as 2.44 (*M. marburgensis'* Mcr's C-H vs. C-D
412 bond-breaking preference, Scheller et al., 2013) to arrive at the actual quantity of activated
413 methane molecules. In this context, the experimental D:^{14}C tracer ratio values may provide useful
414 insight. A D:^{14}C tracer ratio of 2 for the reverse methanogenesis pathway suggests that, for every
415 methane molecule that is fully oxidized to CO_2, two hydrogen atoms enter water-exchangeable
416 intermediates.
417 However, the back reaction of enzymatic processes (Scheller et al., 2010) could lead to
418 heightened D/H ratios in the absence of full carbon oxidation. For example, upon the activation of
419 methane by Mcr, HS-CoB and CH_3-S-CoM form, with the thiol hydrogen exchanging with water-
420 bound hydrogen. If the S-bound hydrogen were deuterium, then the methane re-formed by Mcr
421 back reaction would be CH_4 and the aqueous deuterium would cause a heightened D/H ratio
422 despite a lack of net methane oxidation (Fig. 3). We analyzed the remaining headspace of seep
423 sediment incubations for the formation of CH_4 from CH_3D via ^{1}H-NMR spectroscopy. Over the
424 course of 58 days in triplicate A.Sed-5128 incubations prepared with exclusively CH_3D headspace,
425 CH_4 in the headspace increased from 0.33% +/- 0.02% SE to 4.48% +/- 0.27% SE. If this
426 demonstrated reversibility only reflects the back reaction of Mcr, then the CH_4 increase must be
427 multiplied by four to reflect the actual percentage of headspace methane that was re-formed by
428 Mcr; if the reversibility reflects back reaction of the entire pathway, then no scaling factor is
429 needed. Thus, the range of potential methane headspace percentage accounted for by methane
430 reformed from initial CH_3D is between 4.15 – 16.6%. (For clarity, these calculations neglect

isotope effects and activity by methanogens, factors that can be clarified through further experimentation.) Reversibility can be evaluated in future stable isotope work by a) including a ^{13}C-dissolved inorganic carbon (DIC) signal in the water and measuring $^{13}CH_4$, and/or b) utilizing multiply deuterated methane as initial headspace and quantifying all possible isotopologs. Nonetheless, even the upper bound of partially and reversibly oxidized CH_3D suggests that the majority of the D/H signal is attributable to reactions indicative of net methane consumption, if not complete oxidation.

3.3.2. The D:^{14}C Tracer Ratio in Aerobic Methanotrophy

In aerobic methanotrophic cultures, a D:^{14}C tracer ratio of ~1.5 was observed, suggesting that on average, 2.67 of the four methane-derived hydrogen atoms likely enter water-exchangeable products during the course of a full oxidation pathway. *M. tricosporium* is a type II methanotroph, a member of the *Alphaproteobacteria* that uses the serine pathway for carbon assimilation; *M. sedimenti* is a gammaproteobacterial type I methanotroph, using the RuMP carbon assimilation pathway (Tavormina et al., 2015). The pathway data presented in Fig. 4 suggests that all methane-bound hydrogens are water exchangeable during the catabolic oxidation of methane to carbon dioxide. Thus, to achieve a D:^{14}C tracer ratio less than 4, a substantial proportion of methane-derived formaldehyde would need to proceed down the assimilatory pathway, a requirement that was likely met given the cultures' increase in cell density (data not shown). Intriguingly, the D:^{14}C tracer ratios were similar for both cultured organisms despite their distinct metabolic pathways; a similar phenomenon of consistent carbon conversion efficiency was recently observed among distinct aerobic methanotroph communities in English riverbeds (Trimmer et al., 2015).

The oxic incubations of methane seep sediment produced a D:^{14}C tracer ratio of 1.66 +/- 0.02 SE. Given that the known modes of biological methane oxidation – type I and type II aerobic

methanotrophy and reverse methanogenesis anaerobic methanotrophy – bound this observed value, it appears likely that the oxic sediment incubations supported a mixture of both aerobic and anaerobic methane oxidation processes. Aerobic methane oxidation likely dominated, based on the ~$7x10^4$ Pa partial pressure of O_2 and the proximity of the D:^{14}C tracer ratio to that of the aerobic methanotrophic cultures, but anoxic niches likely remained or developed in the incubation bottles.

3.4. Specialized Application of the Monodeuterated Methane Approach: Anaerobic Methanotrophy at Pressure

To demonstrate the utility of the CH_3D rate measurement approach in addressing experimentally relevant questions, particularly in nontraditional empirical contexts, we sought to evaluate the influence of *in situ* pressure on methanotrophic rates of Hydrate Ridge seep sediment microbial communities. Material collected for microbiological studies of AOM is frequently obtained from marine settings of various depths that are subjected to distinct and substantial pressure regimes (Ruff et al., 2015). Pressure is not always rigorously incorporated into microcosm experiments, though evidence suggests it can be an important determinant of methanotrophic rates (Bowles et al., 2011; Nauhaus et al., 2005; Zhang et al., 2010). In addition, some procedural aspects of the $^{14}CH_4$ protocol, including headspace sampling and full-volume transfer, are not established for use with mylar bags, making the monodeuterated methane approach an appealing alternative in this context.

Parallel seep sediment incubations were subjected to 0.1 MPa (atmospheric pressure) and 9.0 MPa (equivalent to ~900 m depth). δD values derived from heightened D/H ratios attributable to methane consumption, are shown in Fig. 5. A significant increase in methane consumption was observed in both live conditions at heightened pressure, corresponding to sediment incubated with glycine (samples 1a and 1b) and ammonium chloride (samples 2a and 2b). Controls lacking CH_3D

(samples 3a and 3b) and biological activity (samples 4a and 4b) showed no increase in δD (see Table S2 for sample set-up details). The simulation of *in situ* Hydrate Ridge pressures led to a 79.5% (+/- 6.5 SE) increase in relative methane oxidizing rates. Incubation with 500 μM glycine rather than ammonium at high and low pressures resulted in small but consistent rate increases of 12% +/- 4.1% SE, potentially reflecting the energetic and biosynthetic distinction between exogenous amino acids and unprocessed fixed nitrogen.

Previous reports have found a wide range of different pressure-related effects. In a sulfate-coupled AOM bioreactor, pressures were varied from 1 to 8 MPa and sulfide production approximately tripled, demonstrating Michaelis-Menten style kinetics with an apparent K_m of 37 mM (Zhang et al., 2010). Methane partial pressures of 1.1 MPa led to a 5x increase in sulfate reduction rates relative to ambient atmospheric pressure with Hydrate Ridge sediments demonstrating methane-dependent sulfate reduction (Nauhaus et al., 2002). With methane seep sediment from the Japan Trench, however, methane-driven sulfate reduction rates did not correlate with changing pressure (Vossmeyer et al., 2012). Nauhaus et al. (2005) suggested that the pressure-induced rate increases are due more to heightened methane solubility and bioavailability rather than physiological effects or biomolecular re-ordering. Bowles et al. (2011) presented a very different perspective by showing a six- to ten-fold AOM rate increase at 10 MPa when methane concentrations were held constant. Deconvolving these two influences and how they depend on community composition or physicochemical parameters is feasible with pressure chamber experiments utilizing monodeuterated methane. Understanding the relative contributions of environmental and physiological effects to methane oxidation will help constrain methane fluxes across a larger envelope of the planet's methanotrophically active zones.

3.5. Using Monodeuterated Methane in Experimental Investigations

Based on $^{14}CH_4$ ground-truthing experiments with aerobic methanotrophic cultures, oxic seep sediment, and anoxic seep sediment, as well as the proof-of-concept pressurized experiments, we believe that the monodeuterated methane approach to methane oxidation rate measurement is a useful addition to the biogeochemist's tool set. Compared with radiolabel approaches ($^{14}CH_4$, ^{3}H-CH_4, $^{35}SO_4^{2-}$), the method requires less safety-oriented planning, and is logistically simpler, more affordable, and may be less susceptible to hydrogen-associated isotope fractionation effects (relative to ^{3}H). Our results also suggest that the monodeuterated methane technique appears to be a more precise method based on standard error calculations (Figs. 1, 2). Direct comparisons of environmental incubations are complicated by the microheterogeniety of seep settings (Barry et al., 1996; Lloyd et al., 2010), as well as the fact that different aliquots of the same initial material were used in our experiments. However, analysis of culture-based experiments reveals that standard errors from R_{CH3D} values were 20% those derived from $^{14}CH_4$-based values, making the monodeuterated method five times more precise.

Because the monodeuterated methane method focuses on methane-bound hydrogen atoms, it offers different, complementary information about methanotrophic systems than carbon-based techniques like methane or bicarbonate quantification. While this distinction complicates the interpretation of isolated D/H ratios, it can offer an additional dimension of information for analysis of methane-derived intermediates in relevant metabolisms. Given these caveats, we recommend three use cases for monodeuterated methane in methane oxidation rate measurement applications.

1) First, the approach can be employed in a strictly comparative context using analogous inoculum exposed to a range of different conditions, as demonstrated with the pressure-based sediment incubations presented above. Evaluating the effect of different

conditions such as temperature ranges, chemical concentrations, or energetic landscapes on seep sediment methane oxidizing rates would all be promising applications. Comparative analysis of AOM rates at different seep sites would also be useful, provided anaerobic or aerobic methanotrophic processes could be isolated.

2) Second, by performing side-by-side monodeuterated methane and radiocarbon tests, a sample-specific D:^{14}C tracer ratio can be determined, and absolute rates of full methane oxidation can then be inferred in subsequent experiments based exclusively on D/H ratios. Conducting such paired studies under additional environmental or lab-based conditions would help clarify the universality of the ratios presented here and would likely reveal additional questions of metabolic dynamics in a range of experimental systems. We also encourage side-by-side comparisons with other rate measurement approaches, including ^{3}H-CH_4 radiotracer and methane concentration assessments, to develop additional pairwise conversion factors and better constrain carbon and hydrogen metabolism in methane-based biological reactions.

3) Finally, the use of monodeuterated methane as an analytical tool, alongside additional methods such as carbon- or sulfur-tracking procedures, would enable a multi-dimensional examination of anabolic and catabolic processes in methane-based metabolisms. In particular, the D:^{14}C tracer ratios presented here reveal intriguing and seemingly systematic relationships between carbon and hydrogen anabolic and catabolic partitioning across distinct physiologies, yet an underlying theoretical framework regarding the fate of methane-bound hydrogen atoms remains outstanding. In anaerobic methanotrophic systems, back-reaction rates and equilibrium constants could be evaluated by a) including a $^{13}CO_2$ signal in the water and measuring $^{13}CH_4$, and/or b)

utilizing multiply deuterated methane as initial headspace and measuring all possible isotopologues via NMR or high resolution mass spectrometry. For aerobic methanotrophs, evaluating D:^{14}C tracer ratios under more clearly defined growth and maintenance phases would elucidate distinct values associated with catabolic, RuMP, and serine pathways, enabling future use of that parameter as an arbiter of relative anabolic and catabolic activity. Furthermore, additional environmental variables can be tested to gain insight into distinct redox pathways and dynamics of reversibility. For example, AOM under lower sulfate concentrations might be expected to generate higher D:^{14}C tracer ratios (Yoshinaga et al., 2014), and this parameter could be further developed as a measure of microbially mediated isotopic equilibration.

4. Conclusion

The ability to accurately measure methane consumption and oxidation rates – both comparatively and in absolute values – is an important component of methanotrophic studies. Such measurements frequently depend on radiotracers or measurements of chemical species that are related to, but not directly indicative of, methane metabolism. The monodeuterated methane technique presented here represents a novel approach to methane oxidation rate measurements, notable for its logistical and analytical ease (particularly in ship-board applications), as well as the added dimension provided by H-based, rather than C-based, information. We have demonstrated that the D/H ratio is a reliable proxy for methane oxidation activity: in several applications, the value is directly proportional to methane oxidation rates as measured in absolute terms by the well-established $^{14}CH_4$ method. The value of the proportionality constant differs based on the experimental system, likely dictated by environmental variables and the relative proportions of

aerobic and anaerobic methanotrophic metabolisms, though additional experiments to determine the nature of the putative mixing line are needed.

Methane biogeochemistry is a dynamic field of study with implications for carbon cycling, microbial ecology, and climate dynamics, though experimental challenges have slowed our understanding of methane-based biological reactions. With the CH_3D approach as an added tool in the arsenal of rate-based examinations, a broader understanding of the intricacies of methane metabolism, as well as its role in environmental and anthropogenic systems, is within reach.

5. Acknowledgements

We thank the Captains, Crew, *Alvin* group, *Jason* group, and Science party members from *RV Atlantis* legs AT-15-68, and AT-18-10. Water analyzer measurements were conducted in the laboratory of Alex Sessions at the California Institute of Technology with technical support from Lichun Zhang. We are indebted to William Berelson at the University of Southern California and Nick Rollins for use of their pressure chambers and assistance with the incubation experiments. We thank Alex Sessions, Woodward Fischer, Dianne Newman, Tori Hoehler, Amy Rosenzweig, Daniel Stolper, and Linda Reynard for helpful conversations during the preparation of the manuscript. This study was funded by grants from the U.S. Department of Energy, Office of Science, Office of Biological and Environmental Research (DE-SC001057), the NASA Astrobiology Institute (Award # NNA13AA92A) and support from the Gordon and Betty Moore Foundation through grant GBMF3780 (to VJO). JJM was supported by a National Energy Technology Laboratory Methane Hydrate Research Fellowship funded by the National Research Council of the National Academies. This research used resources of the Oak Ridge Leadership

591 Computing Facility. Oak Ridge National Laboratory is supported by the Office of Science of the
592 U.S. Department of Energy.

593

594 6. References

595 Alperin, M. J., and Reeburgh, W. S. (1985). Inhibition Experiments on Anaerobic Methane Oxidation.
596 *Applied and Environmental Microbiology* 50, 940–945.

597 Barry, J. P., Gary Greene, H., Orange, D. L., Baxter, C. H., Robison, B. H., Kochevar, R. E., et al.
598 (1996). Biologic and geologic characteristics of cold seeps in Monterey Bay, California. *Deep Sea*
599 *Research Part I: Oceanographic Research Papers* 43, 1739–1762.

600 Beal, E. J., House, C. H., and Orphan, V. J. (2009). Manganese- and Iron-Dependent Marine Methane
601 Oxidation. *Science* 325, 184–187. doi:10.1126/science.1169984.

602 Boetius, A., Ravenschlag, K., Schubert, C. J., Rickert, D., Widdel, F., Gleseke, A., et al. (2000). A
603 marine microbial consortium apparently mediating anaerobic oxidation of methane. *Nature*
604 407.

605 Boetius, A., and Suess, E. (2004). Hydrate Ridge: a natural laboratory for the study of microbial life
606 fueled by methane from near-surface gas hydrates. *Chemical Geology* 205, 291–310.
607 doi:10.1016/j.chemgeo.2003.12.034.

608 Bowles, M. W., Samarkin, V. A., and Joye, S. B. (2011). Improved measurement of microbial activity in
609 deep-sea sediments at in situ pressure and methane concentration. *Limnology and Oceanography:*
610 *Methods* 9, 499–506.

611 Bussmann, I., Matousu, A., Osudar, R., and Mau, S. (2015). Assessment of the radio 3H-CH4 tracer
612 technique to measure aerobic methane oxidation in the water column. *Limnology and*
613 *Oceanography: Methods* 13, 312–327.

614 Carini, S. A., Orcutt, B. N., and Joye, S. B. (2003). Interactions between methane oxidation and
615 nitrification in coastal sediments. *Geomicrobiology Journal* 20, 355–374.

616 Crespo-Medina, M., Meile, C., Hunter, K., Diercks, A., Asper, V., Orphan, V., et al. (2014). The rise
617 and fall of methanotrophy following a deepwater oil-well blowout. *Nature Geoscience*.

618 Dawson, K., Osburn, M., Sessions, A., and Orphan, V. (2015). Metabolic associations with archaea
619 drive shifts in hydrogen isotope fractionation in sulfate-reducing bacterial lipids in cocultures
620 and methane seeps. *Geobiology* 13, 462–477.

621 Dunfield, P. F., Yuryev, A., Senin, P., Smirnova, A. V., Stott, M. B., Hou, S., et al. (2007). Methane
622 oxidation by an extremely acidophilic bacterium of the phylum Verrucomicrobia. *Nature* 450,
623 879–882.

624 Ettwig, K. F., Butler, M. K., Le Paslier, D., Pelletier, E., Mangenot, S., Kuypers, M. M., et al. (2010).
625 Nitrite-driven anaerobic methane oxidation by oxygenic bacteria. *Nature* 464, 543–548.

626 Gieskes, J., Mahn, C., Day, S., Martin, J. B., Greinert, J., Rathburn, T., et al. (2005). A study of the
627 chemistry of pore fluids and authigenic carbonates in methane seep environments: Kodiak
628 Trench, Hydrate Ridge, Monterey Bay, and Eel River Basin. *Chemical Geology* 220, 329–345.
629 doi:10.1016/j.chemgeo.2005.04.002.

630 Girguis, P. R., Orphan, V. J., Hallam, S. J., and DeLong, E. F. (2003). Growth and Methane Oxidation
631 Rates of Anaerobic Methanotrophic Archaea in a Continuous-Flow Bioreactor. *Applied and*
632 *Environmental Microbiology* 69, 5472–5482. doi:10.1128/AEM.69.9.5472-5482.2003.

633 Hakemian, A. S., and Rosenzweig, A. C. (2007). The biochemistry of methane oxidation. *Annu. Rev.*
634 *Biochem.* 76, 223–241.

635 Hallam, S. J., Putnam, N., Preston, C. M., Detter, J. C., Rokhsar, D., Richardson, P. M., et al. (2004).
636 Reverse methanogenesis: testing the hypothesis with environmental genomics. *Science* 305,
637 1457–1462.

638 Haroon, M. F., Hu, S., Shi, Y., Imelfort, M., Keller, J., Hugenholtz, P., et al. (2013). Anaerobic
639 oxidation of methane coupled to nitrate reduction in a novel archaeal lineage. *Nature* 500, 567–
640 570.

641 Ho, A., Vlaeminck, S. E., Ettwig, K. F., Schneider, B., Frenzel, P., and Boon, N. (2013). Revisiting
642 methanotrophic communities in sewage treatment plants. *Applied and environmental microbiology*
643 79, 2841–2846.

644 Holler, T., Wegener, G., Niemann, H., Deusner, C., Ferdelman, T. G., Boetius, A., et al. (2011).
645 Carbon and sulfur back flux during anaerobic microbial oxidation of methane and coupled
646 sulfate reduction. *Proceedings of the National Academy of Sciences* 108, E1484–E1490.
647 doi:10.1073/pnas.1106032108.

648 Holzapfel-Pschorn, A., Conrad, R., and Seiler, W. (1985). Production, oxidation and emission of
649 methane in rice paddies. *FEMS Microbiology Ecology* 1, 343–351.

650 Huang, M., Hilderman, J. N., and Barbour, L. (2015). Transport of stable isotopes of water and
651 sulphate within reclaimed oil sands saline–sodic mine overburden. *Journal of Hydrology* 529,
652 1550–1561.

653 Jørgensen, B. B., Weber, A., and Zopfi, J. (2001). Sulfate reduction and anaerobic methane oxidation
654 in Black Sea sediments. *Deep Sea Research Part I: Oceanographic Research Papers* 48, 2097–2120.

655 Kirschke, S., Bousquet, P., Ciais, P., Saunois, M., Canadell, J. G., Dlugokencky, E. J., et al. (2013).
656 Three decades of global methane sources and sinks. *Nature Geosci* 6, 813–823.

657 Knittel, K., and Boetius, A. (2009). Anaerobic Oxidation of Methane: Progress with an Unknown
658 Process. *Annu. Rev. Microbiol.* 63, 311–334. doi:10.1146/annurev.micro.61.080706.093130.

659 Lieberman, R. L., and Rosenzweig, A. C. (2004). Biological methane oxidation: regulation,
660 biochemistry, and active site structure of particulate methane monooxygenase. *Critical reviews in*
661 *biochemistry and molecular biology* 39, 147–164.

662 Lis, G., Wassenaar, L., and Hendry, M. (2008). High-precision laser spectroscopy D/H and 18O/16O
663 measurements of microliter natural water samples. *Analytical Chemistry* 80, 287–293.

664 Lloyd, K. G., Albert, D. B., Biddle, J. F., Chanton, J. P., Pizarro, O., and Teske, A. (2010). Spatial
665 structure and activity of sedimentary microbial communities underlying a Beggiatoa spp. mat
666 in a Gulf of Mexico hydrocarbon seep. *PLoS One* 5, e8738.

667 Mackelprang, R., Waldrop, M. P., DeAngelis, K. M., David, M. M., Chavarria, K. L., Blazewicz, S. J., et
668 al. (2011). Metagenomic analysis of a permafrost microbial community reveals a rapid response
669 to thaw. *Nature* 480, 368–371.

670 Magen, C., Lapham, L. L., Pohlman, J. W., Marshall, K., Bosman, S., Casso, M., et al. (2014). A simple
671 headspace equilibration method for measuring dissolved methane. *Limnol. Oceanogr. Methods* 12,
672 637–650.

673 Marlow, J. J., Skennerton, C. T., Li, Z., Chourey, K., Hettich, R. L., Pan, C., et al. (2016). Proteomic
674 Stable Isotope Probing Reveals Biosynthesis Dynamics of Slow Growing Methane Based
675 Microbial Communities. *Frontiers in microbiology* 7.

676 Marlow, J. J., Steele, J. A., Ziebis, W., Thurber, A. R., Levin, L. A., and Orphan, V. J. (2014).
677 Carbonate-hosted methanotrophy represents an unrecognized methane sink in the deep sea.
678 *Nature Communications*.

679 Mau, S., Blees, J., Helmke, E., Niemann, H., and Damm, E. (2013). Vertical distribution of methane
680 oxidation and methanotrophic response to elevated methane concentrations in stratified
681 waters of the Arctic fjord Storfjorden (Svalbard, Norway). *Biogeosciences* 10, 6267–6278.

682 McGlynn, S. E., Chadwick, G. L., Kempes, C. P., and Orphan, V. J. (2015). Single cell activity reveals
683 direct electron transfer in methanotrophic consortia. *Nature* 526, 531–535.

684 Moran, J. J., Beal, E. J., Vrentas, J. M., Orphan, V. J., Freeman, K. H., and House, C. H. (2008). Methyl
685 sulfides as intermediates in the anaerobic oxidation of methane. *Environmental Microbiology* 10,
686 162–173. doi:10.1111/j.1462-2920.2007.01441.x.

687 Nauhaus, K., Boetius, A., Krüger, M., and Widdel, F. (2002). In vitro demonstration of anaerobic
688 oxidation of methane coupled to sulphate reduction in sediment from a marine gas hydrate
689 area. *Environmental Microbiology* 4, 296–305. doi:10.1046/j.1462-2920.2002.00299.x.

690 Nauhaus, K., Treude, T., Boetius, A., and Krüger, M. (2005). Environmental regulation of the
691 anaerobic oxidation of methane: a comparison of ANME-I and ANME-II communities.
692 *Environmental Microbiology* 7, 98–106. doi:10.1111/j.1462-2920.2004.00669.x.

693 Op den Camp, H. J. M., Islam, T., Stott, M. B., Harhangi, H. R., Hynes, A., Schouten, S., et al. (2009).
694 Environmental, genomic and taxonomic perspectives on methanotrophic Verrucomicrobia.
695 *Environmental Microbiology Reports* 1, 293–306. doi:10.1111/j.1758-2229.2009.00022.x.

Pack, M. A., Heintz, M. B., Reeburgh, W. S., Trumbore, S. E., Valentine, D. L., Xu, X., et al. (2011). A method for measuring methane oxidation rates using lowlevels of 14C-labeled methane and accelerator mass spectrometry. *Limnology and Oceanography: Methods* 9, 245–260.

Reeburgh, W. S. (2007). Oceanic Methane Biogeochemistry. *Chem. Rev.* 107, 486–513. doi:10.1021/cr050362v.

Robson, T., and Webb, J. (2016). The use of environmental tracers to determine focused recharge from a saline disposal basin and irrigation channels in a semiarid environment in Southeastern Australia. *Journal of Hydrology* 538, 326–338.

Ruff, S. E., Biddle, J. F., Teske, A. P., Knittel, K., Boetius, A., and Ramette, A. (2015). Global dispersion and local diversification of the methane seep microbiome. *Proceedings of the National Academy of Sciences*, 201421865.

Ruff, S. E., Kuhfuss, H., Wegener, G., Lott, C., Ramette, A., Wiedling, J., et al. (2016). Methane seep in shallow-water permeable sediment harbors high diversity of anaerobic methanotrophic communities, Elba, Italy. *Frontiers in microbiology* 7.

Scheller, S., Goenrich, M., Boecher, R., Thauer, R. K., and Jaun, B. (2010). The key nickel enzyme of methanogenesis catalyses the anaerobic oxidation of methane. *Nature* 465, 606–608.

Scheller, S., Goenrich, M., Thauer, R. K., and Jaun, B. (2013). Methyl-Coenzyme M Reductase from Methanogenic Archaea: Isotope Effects on the Formation and Anaerobic Oxidation of Methane. *J. Am. Chem. Soc.* 135, 14975–14984. doi:10.1021/ja406485z.

Scheller, S., Yu, H., Chadwick, G. L., McGlynn, S. E., and Orphan, V. J. (2016). Artificial electron acceptors decouple archaeal methane oxidation from sulfate reduction. *Science* 351, 703–707.

Scheutz, C., Bogner, J., De Visscher, A., Gebert, J., Hilger, H., Huber-Humer, M., et al. (2009). Microbial methane oxidation processes and technologies for mitigation of landfill gas emissions. *Waste Management & Research*.

Segarra, K. E., Comerford, C., Slaughter, J., and Joye, S. B. (2013). Impact of electron acceptor availability on the anaerobic oxidation of methane in coastal freshwater and brackish wetland sediments. *Geochimica et Cosmochimica Acta* 115, 15–30.

Sivan, O., Antler, G., Turchyn, A. V., Marlow, J. J., and Orphan, V. J. (2014). Iron oxides stimulate sulfate-driven anaerobic methane oxidation in seeps. *Proceedings of the National Academy of Sciences* 111, E4139–E4147. doi:10.1073/pnas.1412269111.

Suess, E., Torres, M., Bohrmann, G., Collier, R., Greinert, J., Linke, P., et al. (1999). Gas hydrate destabilization: enhanced dewatering, benthic material turnover and large methane plumes at the Cascadia convergent margin. *Earth and Planetary Science Letters* 170, 1–15.

Tavormina, P. L., Hatzenpichler, R., McGlynn, S., Chadwick, G., Dawson, K. S., Connon, S. A., et al. (2015). Methyloprofundus sedimenti gen. nov., sp. nov., an obligate methanotroph from ocean

731 sediment belonging to the "deep sea-1"clade of marine methanotrophs. *International journal of*
732 *systematic and evolutionary microbiology* 65, 251–259.

733 Thauer, R. K. (2011). Anaerobic oxidation of methane with sulfate: on the reversibility of the reactions
734 that are catalyzed by enzymes also involved in methanogenesis from CO 2. *Current opinion in*
735 *microbiology* 14, 292–299.

736 Treude, Boetius, Knittel, Wallmann, and Jorgensen (2003). Anaerobic oxidation of methane above gas
737 hydrates at Hydrate Ridge, NE Pacific Ocean. *Mar Ecol Prog Ser* 264, 1–14.

738 Treude, T., Krüger, M., Boetius, A., and Jørgensen, B. B. (2005). Environmental control on anaerobic
739 oxidation of methane in the gassy sediments of Eckernfoerde Bay(German Baltic). *Limnology*
740 *and oceanography* 50, 1771–1786.

741 Treude, T., and Ziebis, W. (2010). Methane oxidation in permeable sediments at hydrocarbon seeps in
742 the Santa Barbara Channel, California. *Biogeosciences (BG)* 7, 3095–3108.

743 Trimmer, M., Shelley, F. C., Purdy, K. J., Maanoja, S. T., Chronopoulou, P.-M., and Grey, J. (2015).
744 Riverbed methanotrophy sustained by high carbon conversion efficiency. *ISME J* 9, 2304–
745 2314.

746 Tryon, M. ., Brown, K. ., and Torres, M. . (2002). Fluid and chemical flux in and out of sediments
747 hosting methane hydrate deposits on Hydrate Ridge, OR, II: Hydrological processes. *Earth and*
748 *Planetary Science Letters* 201, 541–557. doi:10.1016/S0012-821X(02)00732-X.

749 Valentine, D. L., Blanton, D. C., Reeburgh, W. S., and Kastner, M. (2001). Water column methane
750 oxidation adjacent to an area of active hydrate dissociation, Eel river Basin. *Geochimica et*
751 *Cosmochimica Acta* 65, 2633–2640. doi:10.1016/S0016-7037(01)00625-1.

752 Vorholt, J. A., and Thauer, R. K. (1997). The Active Species of "CO2" Utilized by
753 Formylmethanofuran Dehydrogenase from Methanogenic Archaea. *European Journal of*
754 *Biochemistry* 248, 919–924. doi:10.1111/j.1432-1033.1997.00919.x.

755 Vossmeyer, A., Deusner, C., Kato, C., Inagaki, F., and Ferdelman, T. G. (2012). Substrate-specific
756 pressure-dependence of microbial sulfate reduction in deep-sea cold seep sediments of the
757 Japan Trench. *Frontiers in Microbiology* 3, 253. doi:10.3389/fmicb.2012.00253.

758 Wegener, G., Krukenberg, V., Riedel, D., Tegetmeyer, H. E., and Boetius, A. (2015). Intercellular
759 wiring enables electron transfer between methanotrophic archaea and bacteria. *Nature* 526,
760 587–590.

761 Whittenbury, R., Phillips, K., and Wilkinson, J. (1970). Enrichment, isolation and some properties of
762 methane-utilizing bacteria. *Journal of General Microbiology* 61, 205–218.

763 Yoshinaga, M. Y., Holler, T., Goldhammer, T., Wegener, G., Pohlman, J. W., Brunner, B., et al. (2014).
764 Carbon isotope equilibration during sulphate-limited anaerobic oxidation of methane. *Nature*
765 *Geosci* 7, 190–194.

766 Zhang, Y., Henriet, J.-P., Bursens, J., and Boon, N. (2010). Stimulation of in vitro anaerobic oxidation
767 of methane rate in a continuous high-pressure bioreactor. *Bioresource Technology* 101, 3132–3138.
768 doi:10.1016/j.biortech.2009.11.103.

769
770

771 **7. Tables and Figure Captions**

772 Table 1: A summary of the samples used for all experiments conducted in this study. Green boxes
773 indicate that the experiment took place (with all relevant permutations and controls, as described in
774 the text); blank boxes indicate experiments that were not conducted. CH_3D refers to
775 methanotrophic rate experiments using the novel monodeuterated methane technique, while $^{14}CH_4$
776 refers to the radiolabel-based experiments. The three-part codes for samples derived from
777 environmental material refer to active (A) or low-activity (L) sediments (Sed) or carbonates (Carb),
778 along with a sample-specific four-digit serial number.

779

		Oxic		Anoxic	
		CH_3D	$^{14}CH_4$	CH_3D	$^{14}CH_4$
Aerobic Methanotroph Cultures Experiment					
	M. trichosporium				
	M. sedimenti				
Seep Sediment Experiment					
	A.Sed-5128				
	L.Sed-5043				
Seep Carbonate Experiment					
	A.Carb-5305				
	A.Carb-5152				
	L.Carb-5028				
Pressure Experiment					
	A.Sed-3450				

780
781

782 Table 2: D:^{14}C tracer ratios for the experimental treatments addressed in this study.

783

Aerobic Methanotroph Cultures		
	Exponential Phase	Stationary Phase
M. trichosporium	1.5	1.48
M. sedimenti	1.54	1.59
Methane Seep Sediments and Carbonates		
	Oxic Incubations	Anoxic Incubations
A.Sed-5128	1.62	2.05
L.Sed-5043	1.71	2.01
A.Carb-5305	1.65	1.96
A.Carb-5152	1.63	2.08
L.Carb-5028	1.69	1.86

784

785

786 Fig. 1: Amount of methane consumed over time for cultures of a) the type II methanotroph *M.*
787 *trichosporium* and b) the type I methanotroph *M. sedimenti* using C_{corr} (values derived from the
788 CH_3D method, shown with circles) and the $^{14}CH_4$ method (diamonds), calculated as discussed in
789 the text. $^{14}CH_4$-derived data conveys values of methane consumption and full oxidation, while
790 CH_3D-derived data provides a measure of methane consumption. Error bars show standard errors
791 for three biological replicates, with the exception of the $^{14}CH_4$ –derived killed control (n=1).
792 Obscured data points exhibited values between -60 and 110 nmol for a) and 0 and 60 nmol for b).

793

794 Fig. 2: Methanotrophy in a) oxic and b) anoxic incubations of active and inactive seep sediment
795 and carbonate rocks (n=3 in all cases). Values compare methane consumption / full oxidation rates
796 derived from $^{14}CH_4$ measurements (blue) and methane consumption rates derived from the CH_3D
797 approach (green, R_{CH3D} values). Standard error bars are provided.

798

799 Fig. 3: A schematic diagram demonstrating the potential fate of methane-associated hydrogen
800 atoms in the “reverse methanogenesis” pathway. Hydrogen atoms are distinguished by color and
801 superscript number, and potential exchanges with inter- and intra-cellular water are shown.

802 Potentially detectable methane-derived hydrogen atoms (4, occurring throughout the oxidation
803 pathway) and carbon atoms (1, requiring full oxidation) are highlighted in orange and purple
804 boxes, respectively. Shorter "backflux" arrows reflect the observation that all enzymes (Thauer,
805 2008) and the entire pathway (Holler et al., 2011) have been shown to be reversible. For figure
806 simplicity, isotopically distinct backflux products and cofactor involvement in backflux reactions
807 are not shown. The extended dashed line represents the cell membrane.
808
809 Fig. 4: A schematic diagram demonstrating the potential fate of methane-associated hydrogen
810 atoms in the aerobic methanotrophy pathways. Hydrogen atoms are distinguished by color and
811 superscript number; asterisks represent location-specific ambiguity. Potentially detectable
812 methane-derived hydrogen atoms and carbon atoms are highlighted in orange and purple boxes,
813 respectively. Mmo enzymes are not believed to perform reversible reactions.
814
815 Fig. 5: Pressure experiment results showing water δD values with standard error bars of seep
816 sediment samples following 38-day incubations with CH_3D at 9.0 MPa (brown bars, "b" samples)
817 or 0.1 MPa (pink bars, "a" samples). Additional details on sample treatments can be found in Table
818 S2.

Figure 1

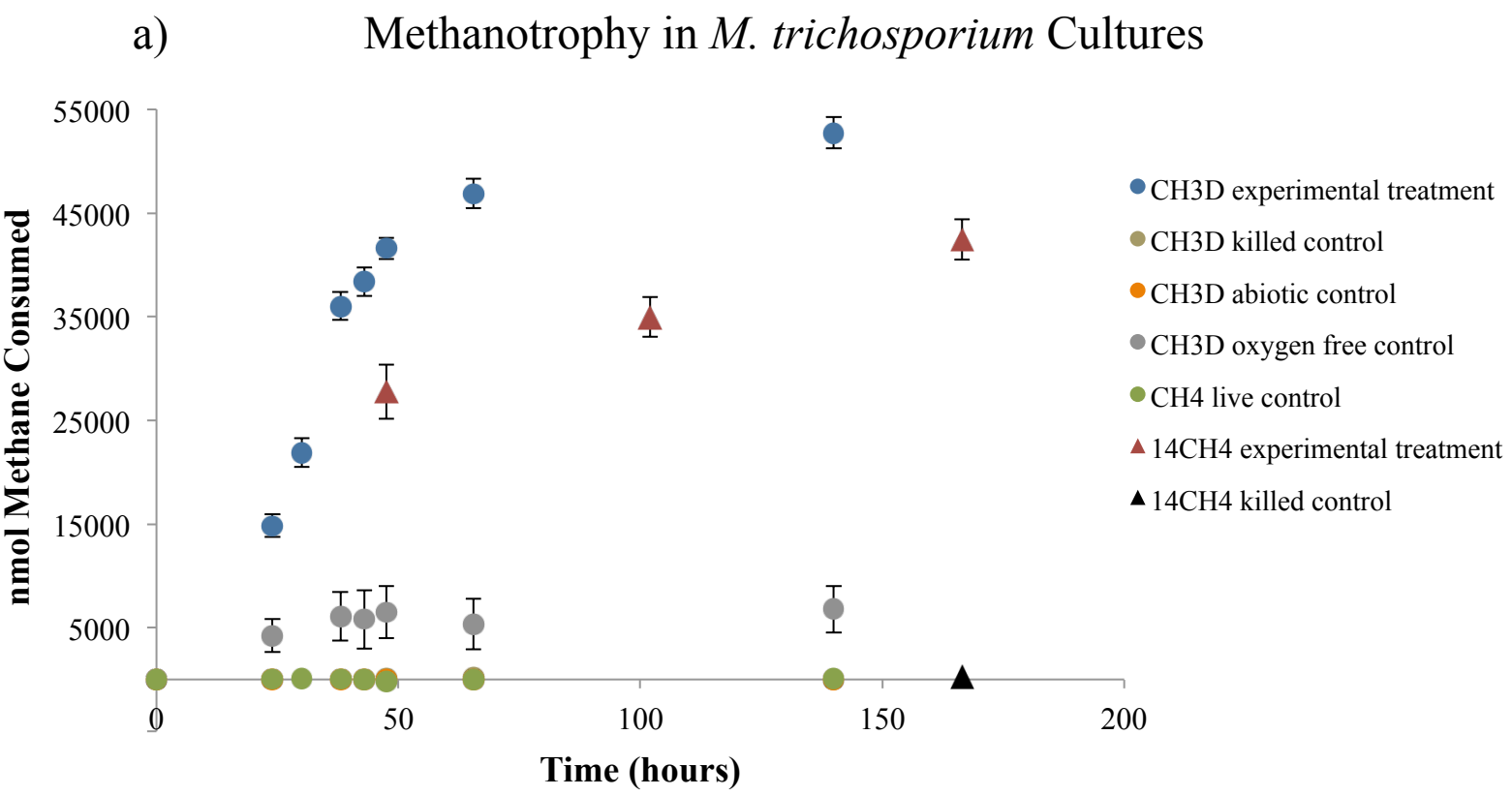
a)
Methanotrophy in *M. trichosporium* Cultures
nmol Methane Consumed
55000
45000
35000
25000
15000
5000
0
50
100
150
200
Time (hours)
CH3D experimental treatment
CH3D killed control
CH3D abiotic control
CH3D oxygen free control
CH4 live control
14CH4 experimental treatment
14CH4 killed control

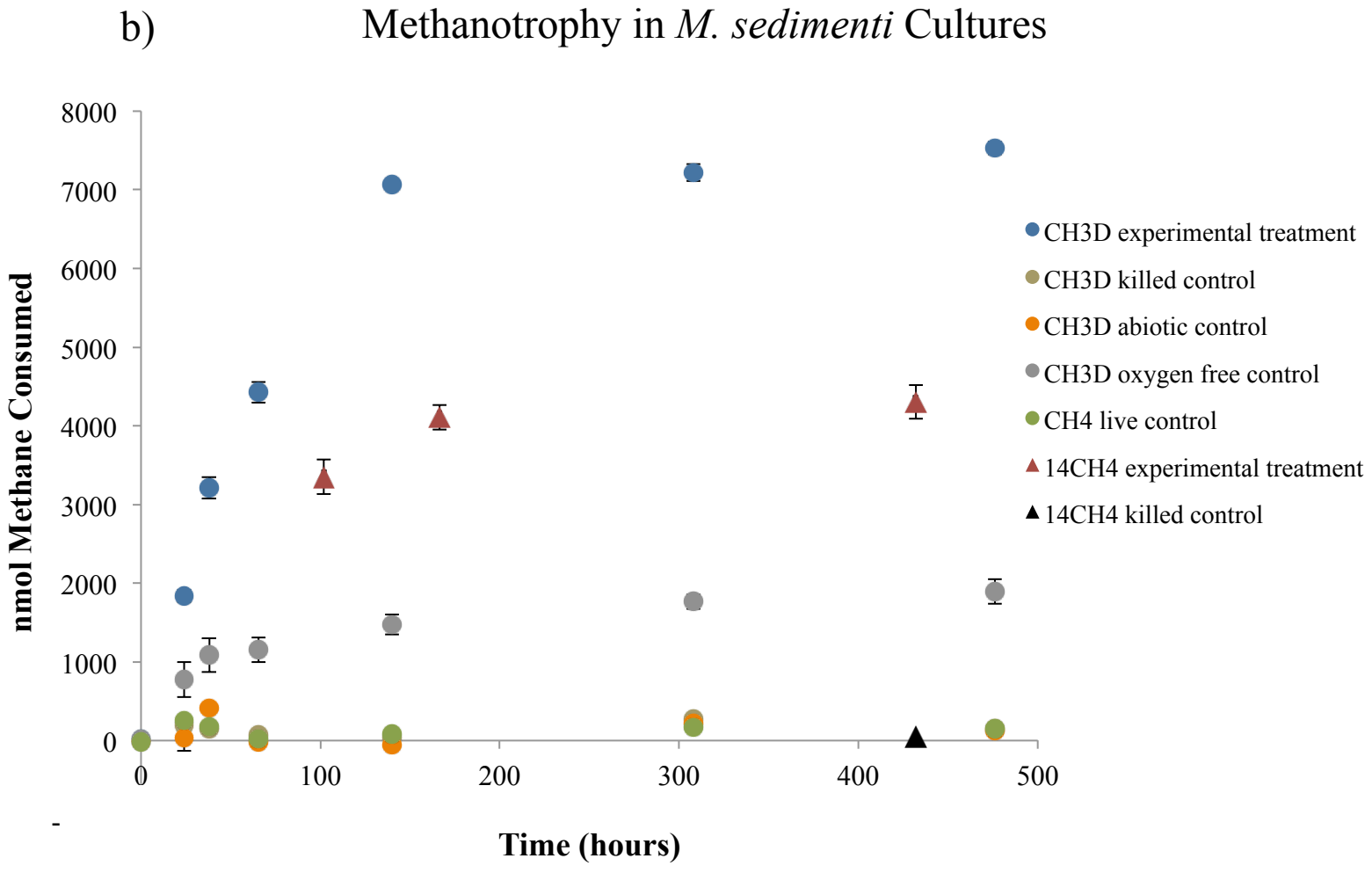
b)
Methanotrophy in *M. sedimenti* Cultures
nmol Methane Consumed
8000
7000
6000
5000
4000
3000
2000
1000
0
100
200
300
400
500
Time (hours)
CH3D experimental treatment
CH3D killed control
CH3D abiotic control
CH3D oxygen free control
CH4 live control
14CH4 experimental treatment
14CH4 killed control

-

Figure 2

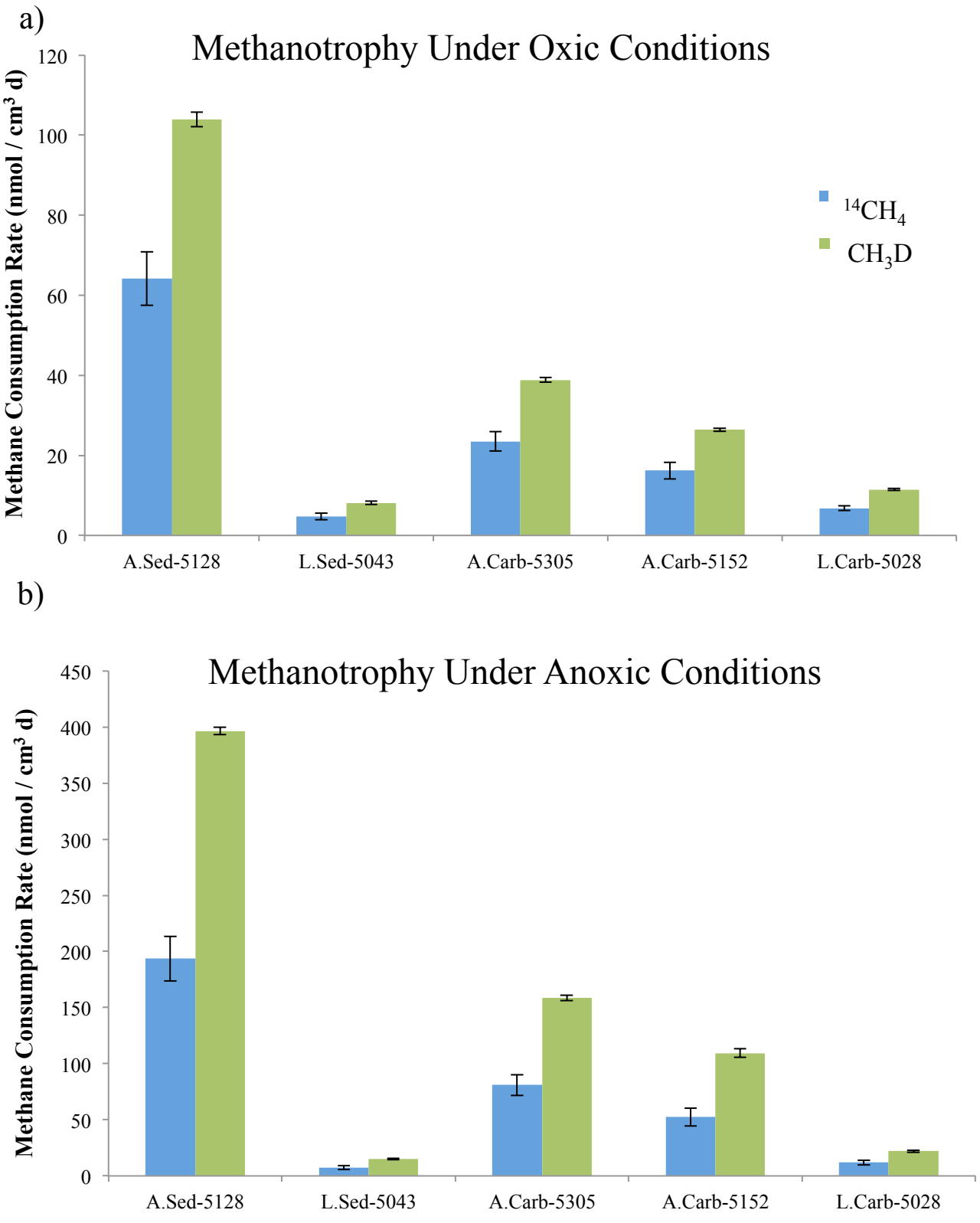
a)
Methanotrophy Under Oxic Conditions
Methane Consumption Rate (nmol / cm³ d)
120
100
80
60
40
20
0
14CH4
CH3D
A.Sed-5128
L.Sed-5043
A.Carb-5305
A.Carb-5152
L.Carb-5028
b)
Methanotrophy Under Anoxic Conditions
Methane Consumption Rate (nmol / cm³ d)
450
400
350
300
250
200
150
100
50
0
A.Sed-5128
L.Sed-5043
A.Carb-5305
A.Carb-5152
L.Carb-5028

Figure 3

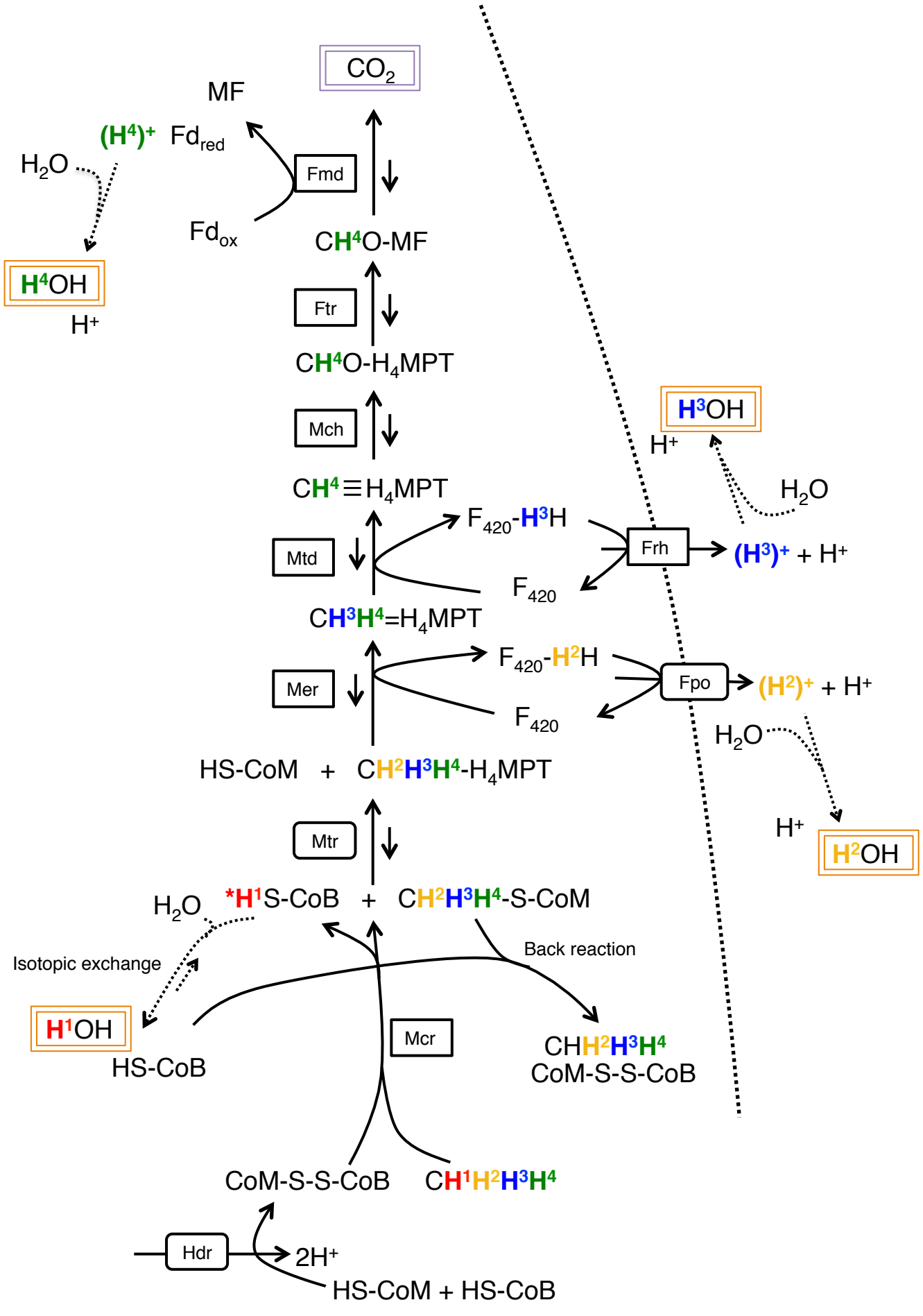
"Reverse Methanogenesis" Pathway
CO_2
MF
$(H^4)^+$ Fd_{red}
H_2O
Fmd
Fd_{ox}
CH^4O-MF
H^4OH
H^+
Ftr
CH^4O-H_4MPT
Mch
$CH^4 \equiv H_4MPT$
H^3OH
H^+
H_2O
F_{420}-H^3H
Mtd
Frh
$(H^3)^+ + H^+$
F_{420}
CH^3H^4=H_4MPT
F_{420}-H^2H
Mer
Fpo
$(H^2)^+ + H^+$
F_{420}
H_2O
HS-CoM + $CH^2H^3H^4$-H_4MPT
H^+
H^2OH
Mtr
H_2O
*H^1S-CoB + $CH^2H^3H^4$-S-CoM
Back reaction
Isotopic exchange
H^1OH
HS-CoB
Mcr
$CHH^2H^3H^4$
CoM-S-S-CoB
CoM-S-S-CoB
$CH^1H^2H^3H^4$
Hdr
$2H^+$
HS-CoM + HS-CoB

Figure 4

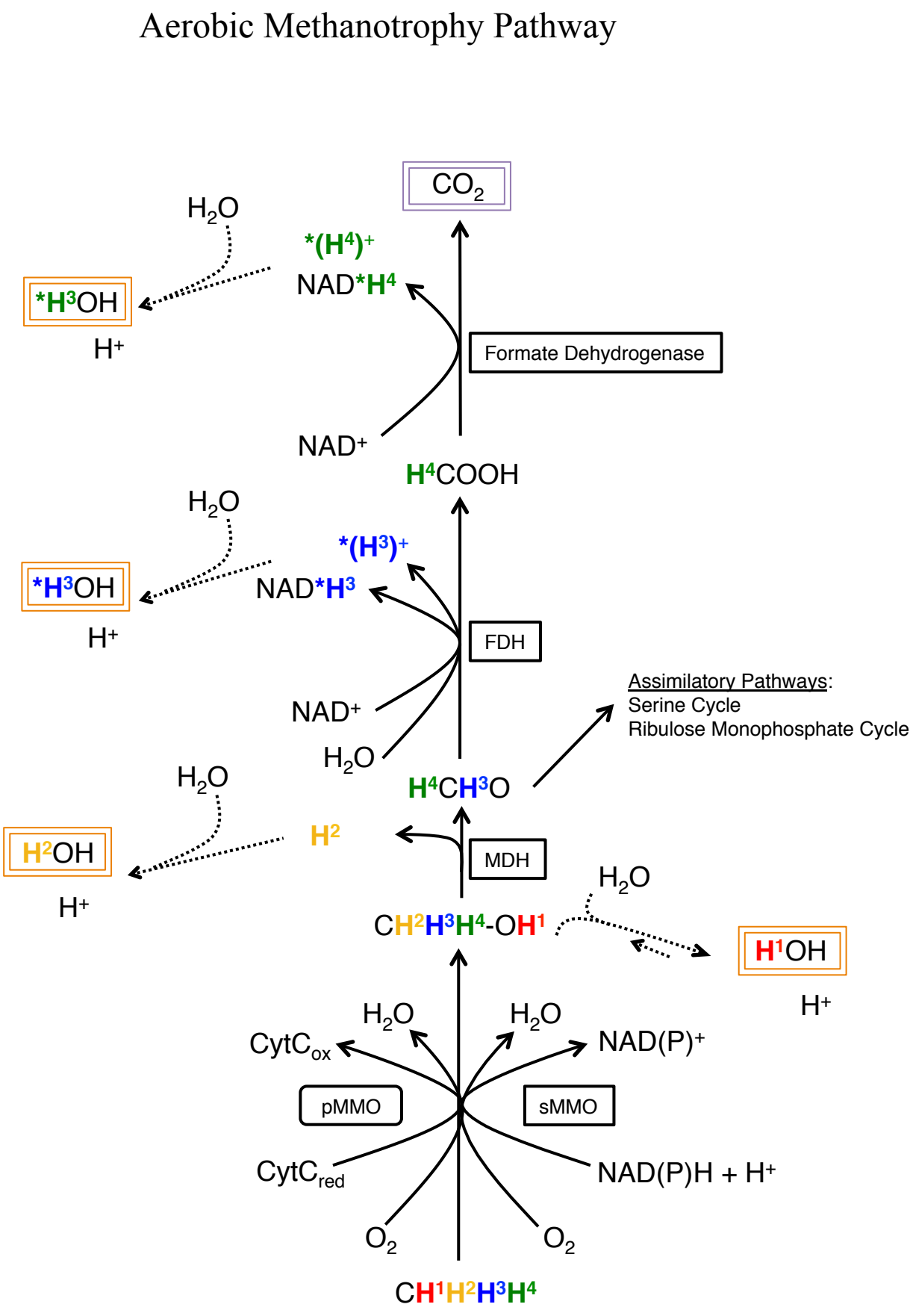
Aerobic Methanotrophy Pathway
CO_2
H_2O
$*(H^4)^+$
$NAD*H^4$
$*H^3OH$
H^+
Formate Dehydrogenase
NAD^+
H^4COOH
H_2O
$*(H^3)^+$
$NAD*H^3$
$*H^3OH$
H^+
FDH
NAD^+
H_2O
Assimilatory Pathways:
Serine Cycle
Ribulose Monophosphate Cycle
H^4CH^3O
H_2O
H^2
H^2OH
H^+
MDH
H_2O
$CH^2H^3H^4\text{-}OH^1$
H^1OH
H^+
H_2O
H_2O
$CytC_{ox}$
$NAD(P)^+$
pMMO
sMMO
$CytC_{red}$
$NAD(P)H + H^+$
O_2
O_2
$CH^1H^2H^3H^4$

Figure 5

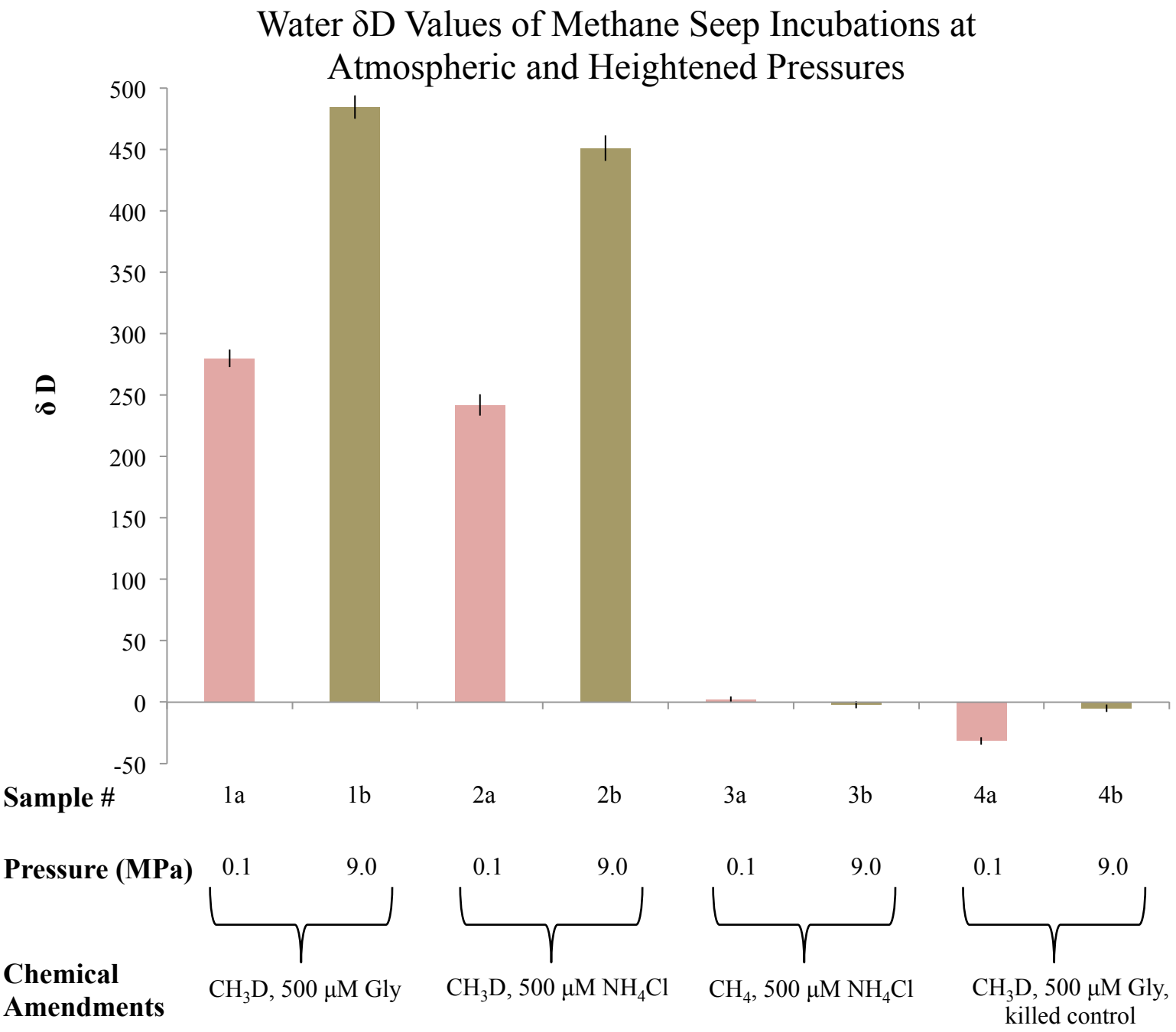
Water δD Values of Methane Seep Incubations at Atmospheric and Heightened Pressures
δ D
500
450
400
350
300
250
200
150
100
50
0
-50
Sample #
1a
1b
2a
2b
3a
3b
4a
4b
Pressure (MPa)
0.1
9.0
0.1
9.0
0.1
9.0
0.1
9.0
Chemical Amendments
CH3D, 500 µM Gly
CH3D, 500 µM NH4Cl
CH4, 500 µM NH4Cl
CH3D, 500 µM Gly, killed control

Figure S1

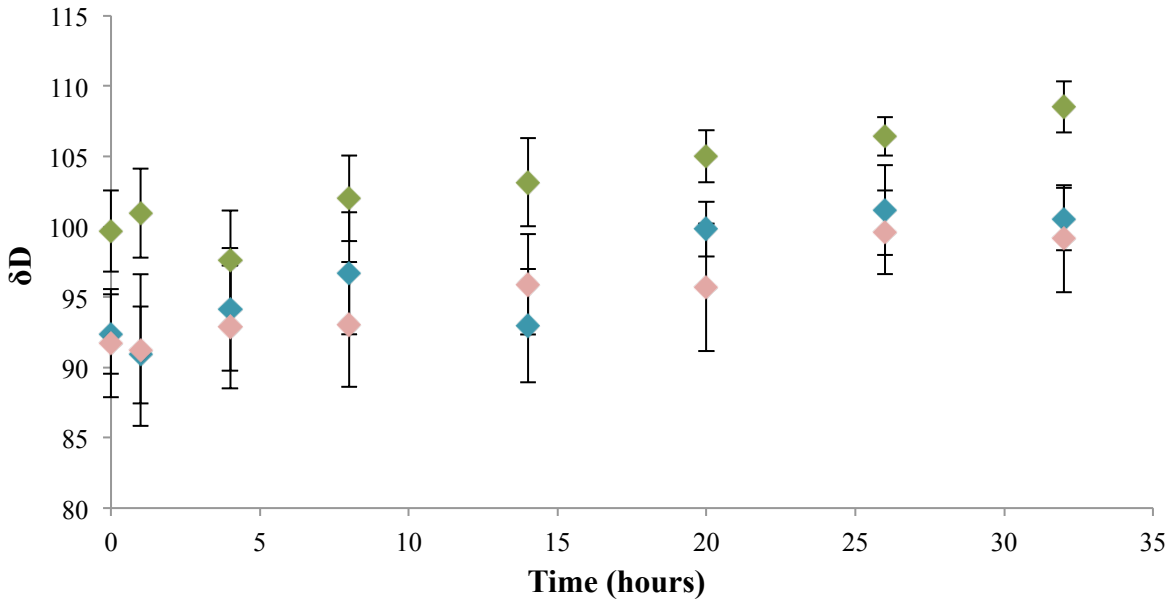

Supplementary Material for "**"Monodeuterated Methane: An Isotopic Probe to Measure Biological Methane Metabolism Rates and Track Catabolic Exchange Reactions"**

Table S1: Conditions for the aerobic methanotrophy experiments. All sample types were set up in triplicate; pressures shown as partial pressures.

Sample Condition	p(CH_3D)	p(CH_4)	$^{14}CH_4$	p(O_2)	p(Ar)	Inoculum Introduced	Killed Cells
1	0.1 MPa			1 x 10^5 Pa		10% v/v	
2	0.1 MPa			1 x 10^5 Pa		10% v/v	Yes
3	0.1 MPa			1 x 10^5 Pa			
4	0.1 MPa				1 x 10^5 Pa	10% v/v	
5		0.1 MPa		1 x 10^5 Pa		10% v/v	
6	0.1 MPa		13 kBq (T1)	1 x 10^5 Pa		10% v/v	
7	0.1 MPa		13 kBq (T2)	1 x 10^5 Pa		10% v/v	
8	0.1 MPa		13 kBq (T3)	1 x 10^5 Pa		10% v/v	
9	0.1 MPa			1 x 10^5 Pa		10% v/v	
10	0.1 MPa		13 kBq (T3)	1 x 10^5 Pa		10% v/v	Yes

Table S2: The experimental set-up for methane seep sediment pressurized rate measurement incubations. The samples ran for 38 days at 4 °C, and each sample was contained in a sealed Mylar bag. Pressure values indicate absolute pressure exerted on the incubated Mylar bags.

Sample #	**Sediment**	**Nitrogen Source**	**Methane Source**	**Pressure (MPa)**
1a	50 mL	500 uM Glycine	40 mL CH_3D	0.1
2a	50 mL	500 uM NH_4Cl	40 mL CH_3D	0.1
3a	50 mL	500 uM NH_4Cl	40 mL CH_4	0.1
4a	50 mL, killed control	500 uM Glycine	40 mL CH_3D	0.1
1b	50 mL	500 uM Glycine	40 mL CH_3D	9.0
2b	50 mL	500 uM NH_4Cl	40 mL CH_3D	9.0
3b	50 mL	500 uM NH_4Cl	40 mL CH_4	9.0
4b	50 mL, killed control	500 uM Glycine	40 mL CH_3D	9.0

Fig. S1: To assess the empirical resolving power of the D/H measurement technique, we determined the time points showing non-overlapping confidence intervals for triplicate incubations of A.Sed-5128. Distinct signals were seen at the 20-hour time point for replicate A (teal diamonds) and the 26-hour time point for replicates B (pink diamonds) and C (green diamonds).